First-principles potentials in modeling structure and thermodynamics of Fe-Ni alloys

H.-P. Cheng and D. E. Ellis
Department of Physics and Astronomy and Materials Research Center, Northwestern University, Evanston, Illinois 60208
(Received 29 December 1988)

First-principles local-density-functional (LD) calculations on small clusters were used to construct interaction potentials for iron and iron-nickel systems. The effective pair potential ϕ_{ij} of the semiempirical embedded-atom method (EAM) was adopted for Ni-Fe and Fe-Fe interactions using differences: $\Delta\phi^{\mathrm{LD}}=\Delta\phi^{\mathrm{EAM}}$ and the Ni-Ni potential of Daw *et al.* The density-dependent embedding-energy function $F(\rho)$ of Fe was adjusted to conform to known scaling laws. The calculation of LD pair potentials was carried out for a number of $\mathrm{Fe}_m\mathrm{Ni}_n$ clusters to determine suitable procedures for extracting ϕ. The effective potentials thus determined were applied to bulk and Fe-Ni alloys in molecular-dynamics simulations to determine equilibrium surface and bulk structures, and thermodynamical properties. The calculated bulk properties of Ni satisfactorily reproduce previous simulation results and experiment; those of bcc iron agree fairly well with experimental results. Moreover, certain properties such as vacancy-formation enthalpies are sufficiently sensitive to be useful in guiding further refinement of the potential.

I. INTRODUCTION

Over the past several decades the volume of scientific research on transition metals and alloys has been growing rapidly. Both theorists and experimentalists are seeking a basic understanding of the properties that make materials useful that goes beyond the traditional metallurgy perspective to a more atomistic view.[1] The great value of such materials in present manufacturing technology as well as in the laboratory and the potential for the future is evident; consequently, their electronic structure and temperature-dependent dynamic properties are of fundamental interest. Advances in modern technology and metallurgy have provided many ways to probe electronic structures: energy-level spectroscopies, melting and crystallization studies, defect structures and migration, and so on.[2] Both experimental measurements and calculations based on theoretical models have already attained a good degree of precision at the spectroscopic level. However, comparison between experimental bulk properties at finite temperature and first-principles theory is not common.

The substantial difficulties encountered in transition-metal (TM) studies are due to their complex electronic structure, due largely to interactions among the d electrons. Many-body cluster expansions of TM bulk properties apparently converge relatively slowly because of the electron correlation in these systems; at least it is generally understood that two-body potentials alone are inadequate. In quantum theory, the many-electron interactions in solid-state systems are traditionally dealt with either by the Green's-function method,[3] which becomes intractable as the number of particles increases, or by solving single-particle Schrödinger equations with a self-consistent effective potential. The latter is based on mean-field theory with well-known approximations derived from density-functional (DF) or, alternatively, by Hartree-Fock theory. The DF theory is usually used in conjunction with the local-density approximation (LDA) of Kohn and Sham[4] and provides much insight of transition-metal electronic structure including spectroscopic, cohesive, and magnetic properties at zero temperature. The advantages of DF theory over other theories, e.g., the Hartree-Fock method, concern approximations to both exchange and correlation energy, which then permit practical application to multiatom systems with the LD approach. The total-energy estimation in DF theory has been successfully used to determine the crystal structure of both crystals and clusters of transition metals.

Physical methodology focusing on atom-level behavior has penetrated into metallurgy as well as many other fields. On one hand, first-principles calculations by both band-structure and cluster methods mentioned above are evidently powerful in determining the bulk, surface structure, and magnetic properties for virtually all metals in the Periodic Table and their alloys at $T=0$ K. On the other hand, it has been long realized that there is a tremendous gap between the quantum theory which typically deals with systems of high symmetry and the experimental observation which reflects finite-temperature effects with accompanying thermal disorder. The computer time consumed in quantum-mechanical calculations increases considerably as the symmetry is lowered and the size of the basic unit considered is increased. Even for the simple metals, it is not very promising to calculate geometry-dependent properties of low-symmetry systems in detail with more than, say, five atoms in the cluster. It is more forbidding for transition metals.

Nevertheless, computer-simulation methods based upon classical Newtonian mechanics provide a good tool to fill the big gap between experimental activities and theoretical descriptions. There is a tremendous amount of existing research on the computer simulation of vari-

ous perspectives of metallurgy, including surface diffusion, interface diffusion, interface free energies, brittle fracture, and phase transitions.[5] Computer-simulation and, particularly, molecular-dynamics (MD) methods are thus widely adopted for modeling "realistic" problems at macroscopic time and distance scales. At this stage a classical model is adopted and the principal problems are concerned with the determination of the potential-energy function. The resulting demand for good model potentials which can describe real physical phenomena quantitatively or even qualitatively leads to a search for more rigorous methods.

The search for parameters defining potential-energy surfaces is an arduous task.[6] Enormous efforts have been made to explore the geometries associated with the degrees of freedom for a system with few ($N=3-6$) atoms. In general, different experiments give information about different parts of the surface, and a particular *ab initio* technique may have different levels of accuracy for different parts of the surface. It is still a major problem to gather all available information into a functional representation which can be used in computer simulations. For a large system, to obtain the entire potential surface geometry is not feasible with present and foreseeable future experimental techniques. Computer size and speed limitations dictate that various severe approximations have to be made to obtain theoretical information on the surface regions of interest. In crystalline material studies the interactions between atoms are usually chosen to fit force constants, bond lengths and cohesion, and lattice vibration frequencies, usually in pairwise-potential form.

When cluster size is not very big, say, 3–10 atoms, the number of independent coordinates is reduced in comparison to the bulk system. However, the difficulties still are serious, with no well-developed methodology. This is a matter of concern since the small clusters are largely relevant to processes controlling chemical reactions, catalysis, melting behavior, and so on. In these phenomena the energy surface is crucial in determining atomic trajectories, e.g., in catalytic process small details of the surface may play an extremely important role in determining the whole direction of reaction. Over the whole Periodic Table there are only a few elements, essentially the inert gases, for which the interatomic interactions are known to be essentially pairwise. The success of pairwise models is understood to depend upon weak electron-electron correlation. However, efforts made in the investigation of complex materials such as transition metals have revealed the need for more complex interaction models.

At this stage, first-principles calculations have been successful in describing some static properties, and occasionally a temperature-dependence of some parameters. For example, under density-functional (DF) theory, the equilibrium bulk and surface structures, cluster bond lengths, and binding energies have been described for a number of TM systems.[7] The binding-energy–curve calculations, however, are mostly limited to bulk uniform dilation in the solid state and dimer bond lengths in clusters. Thus the vast majority of the potential surface remains to be parametrized, explored, and understood. The embedded-atom method (EAM) is just one of several models being developed to satisfy that requirement.

In this paper we present a simplified method of constructing potential surfaces, using both first-principles calculations and semiempirical data. In the EAM scheme we develop a method of constructing a potential-energy function of metal B from the potential energy of metal A. The principal assumption is that a quantum-mechanical potential can be used to provide a differential correction to the empirical potentials, and if the metal-A potential has been optimized to fit experiment, a fair degree of error cancellation will take place. Various possible choices of the quantum-mechanical pair potential are discussed in order to give a reasonable description of the pairwise interaction in the many-particle environment. With this method a potential-energy function of α-Fe is deduced from the known fcc Ni EAM potential, along with the calculated Fe-Ni interaction. We apply these functions to MD simulations on bulk, surfaces, monolayer films, and dilute alloys. Data on the Fe bulk properties and nickel bulk and film system are compared with the experimental results as a general test of the model potentials. Equilibrium geometry of Fe clusters in bulk nickel, cluster structure on a Ni surface, and the alloy phase for some dilute Fe-Ni systems are investigated. Surface relaxation and clustering are detected for Fe-covered low-index Ni surfaces.

II. METHOD

A. Embedded-atom method

Recognizing the difficulties in finding an accurate explicit representation of the interatomic interaction, an alternate method, the embedded-atom method (EAM), has been developed to estimate the energy of adding an atom to a host by considering it to be immersed in an electron gas of density $n(r)$. The EAM is based on the idea of a quasiatom, or effective medium, as originally suggested by Nørskov and Lang,[8] and by Stott and Zaremba.[8] In this model, the whole atom, nucleus or ion and its electron polarization cloud, is considered as a single unit or "quasiatom" analogous to the concept of the quasiparticle in liquid-helium theory. Since the ion or nucleus is shielded by the electron cloud, it appears neutral at a certain distance and is unaffected by the charge distribution beyond a certain region. Instead of focusing upon orbital-by-orbital electronic response as in the pseudopotential theory, the EAM concentrates on the "host," the effective medium and its influence on the entire atom. The key parameter which affects the atom is identified as the charge-density distribution of the host system. In other words, the energy change caused by the presence of an extra atom is predetermined by the undisturbed system,

$$\Delta E=\mathcal{F}_{Z,R}(n_h(r)) \ . \tag{1}$$

In Eq. (1), $\mathcal{F}$ stands for a functional of the density, the subscripts Z,R are the atomic number and the coordinates of the immersed atom, and h represents the host. It is important to understand that the Stott-Zaremba hypothesis [Eq. (1)] is not a means of solving for the self-

consistent density distribution of the entire system as implied by the Hohenberg-Kohn theorem. Rather, it is a model based on the self-consistent calculation which is therefore done implicitly.

The concept of a quasiatom provides a promising approach in estimating the energy of an atom which is immersed in a host. In the application to metal or alloy systems, the method can be used to calculate the total energy by viewing each atom in the system as an impurity and the total energy as simply the summation of all embedding energies, i.e.,

$$E_{\rm tot}=\sum_i F_i(\rho_{h,i}) \ . \tag{2}$$

The embedding energy $F_i(\rho_{h,i})$ in Eq. (2) is not trivially related to the immersion energy defined in Eq. (1) as pointed out by Daw and Baskes.[9] However, careful consideration shows F differs from $\mathcal{F}$ only in the different ways of presenting the total energy. Therefore we use the same terminology "embedding energy" to represent both. Daw and Baskes suggested[9] a modified scheme to improve the total-energy expression:

$$E_{\rm tot}=\tfrac{1}{2}\sum_{\substack{i,j\\(i\neq j)}}\phi_{ij}(r)+\sum_i F_i(\rho_{h,i}) \ . \tag{3}$$

The meaning of ϕ_{ij} in Eq. (3) is straightforward: it is the effective two-body interaction between atoms. The purpose of this additional term is to include the effects responsible for deviations from the uniform-density jellium model. For complicated systems like transition metals, the uniform-density approximation (UDA), and low-order corrections really do not provide a satisfactory approach. The price which we have to pay in order to use Eq. (3) is to choose a proper pair potential and embedding energy by some other criteria. It is obvious that there is no unique way to separate the two terms from rigorous theoretical considerations. However, empirical forms of ϕ and F can be obtained by fitting the calculated physical properties to the experimental data.[10–13] One can see from the global fitting processes used that the choice of proper ϕ and F is somewhat arbitrary.

For example, once the form of ϕ is chosen, F can be determined by the empirical universal scaling relation for transition metals,[14]

$$E(a^*)=-E_{\rm sub}(1+a^*)e^{-a^*} \ , \tag{4}$$

where $E_{\rm sub}$ is the absolute value of the sublimation energy at zero temperature defined as the energy per atom needed to separate the lattice atoms from their equilibrium positions to infinity. Also, in Eq. (4) the scaled lattice constant is defined as

$$a^*=(a/a_0-1)/(E_{\rm sub}/9B\Omega)^{1/2} \ , \tag{5}$$

where a_0 is the experimental lattice constant, B is the bulk modulus, and Ω is the volume per atom. With this definition $E(a)$ is the energy per atom required to remove all atoms from their lattice points (with lattice constant a) to infinity.

In applications, the argument of F is the total host electron density at the position of the embedded atom. Furthermore, as a plausible ansatz, ρ is chosen as the summation of overlapping spherically averaged atomic charge densities of the system. In the case of a system with slowly varying density, this is a reasonable approximation. This approximation decouples the complex many-body energy to the simple two-body interaction energy plus mean-field form and causes no substantial increase in the time required for MD simulations.

The bulk properties commonly used in generating potential parameters include lattice constant a_0, sublimation energy $E_{\rm sub}$, bulk modulus B, elastic constants $\{C_{ij}\}$ and the vacancy-formation energy E_v^f. With this information, potential parameters have been determined for most fcc transition metals, including Ni, Cu, Pd, Ag, and Pt.[9] It is known in general that EAM works well for fcc transition metals and remains controversial in describing bcc transition metals.[15]

B. First-principles corrections to EAM potential

In this section, we introduce a method developed from cluster calculations by LD quantum theory to construct new potential functions from the known and tested empirical potential functions. To achieve this goal, we make one simple assumption:

$$\Delta\phi_{AB}^{\rm EAM}=\Delta\phi_{AB}^{\rm LD} \ , \tag{6}$$

where ϕ is the pair-potential function. The superscript represents the method by which ϕ is obtained; the subscript indicates different elements A,B and Δ refers to the difference of the pair potential. Equation (6) states that the differences of pair potentials between material A and B in the EAM and LD schemes are equal to each other. This assumption introduces nothing new to the EAM model since the pair potential concerned in the EAM is certainly not assumed to be the "bare" dimer potential. The task remaining is choice of a reasonable procedure to select effective pair potentials from the LD scheme.

One straightforward selection is the LD dimer potential since it completely represents a certain two-body interaction rather accurately. However, our application of the dimer potential in the EAM gives overestimates of the two-body interactions in bulk simulations in the sense of the "energy per bond," the vacancy-formation energy being much bigger than experimental results. This is hardly surprising in view of the many-body screening effects in the bulk. Searching for other possible representations of the effective pair potentials, we have studied triatomic and tetrahedral clusters which could describe pair interactions within some more realistic metallic environment.[16] We may thus improve upon the ϕ part of the EAM model, and this searching process can be continued until we hit upon a (hopefully general) potential which satisfactorily reproduces the physical properties of interest. We apply the proposed potentials in computer simulations on TM solids and films to evaluate their effectiveness in reproducing dynamical and thermodynamic properties.

Once we choose a ϕ, for example, using the effective pair potential from tetrahedral clusters, the present deter-

mination of the $F(\rho)$ function is simple. We use the observed universality of the metal cohesive energy $E(a)$ as described in Eq. (4) and obtain $F(\rho)$ by a process of subtraction, using Eq. (3), keeping in mind that within EAM theory, both F and ϕ are short-range energy terms. The required total charge density ρ of the host at position r is taken as the sum of atomic charge densities $\sum_i \rho_v(\mathbf{r}-\mathbf{R}_i)$ at the reference point. Decoupling the total charge density into the sum of atomic charge densities makes the problem simple, and is physically reasonable if we can determine the effective atomic configuration by independent (static) cluster or band-structure calculations, or experiment. Lacking this possibility, we may calculate the ρ of an atom in a square well by atomic LD methods to simulate the crystal environment and at the same time leave the parameters of the potential well adjustable. For example, if one is interested in improving a surface potential function, there is some freedom to determine the charge-density distribution function for different layers.

III. RESULTS

A. Simulation on bulk Ni and Ni surfaces

The first subject in our simulation is the pure-nickel metal. The potential used is that produced by Daw *et al.*[11] and used by them in MD simulations. There are two major reasons for repeating the simulation process.

(i) We wish to check the reliability of our choice of potential functions as well as the validity of the Gibbsian dynamics[17] used in these calculations.[18] We use both direct temperature renormalizations and "variable-s" method (Gibbsian dynamics) and find that the results are consistent with each other.

(ii) The nickel potentials, precisely fitted to extensive experimental data, provide good starting potentials which can be use to generate potentials for other metals, e.g., iron.

The number of atoms in the MD cell was taken to be 256, corresponding to four fcc crystal cells in each direction of three-dimensional space. The temperature was kept at 20 K for calculating the cohesive energy and lattice constant and 300 K for most of the other properties under investigation. The constant-pressure specific heat C_p is measured from the energy-temperature relation. The pressure is chosen to be zero.

In Table I we give the values from our calculations along with experimental data on the bulk nickel properties. One sees that our data essentially reproduce the experimental results. The cohesive energy E_b, defined by energy per atom needed to separate all atoms to infinity, the lattice constant a_0, vacancy-formation energy (we refer to the energy here and in following sections as enthalpy) E_v^f, which is the energy needed to generate a vacancy in crystal, the vacancy-migration energy E_v^m, defined as the energy needed for an atom to jump into a vacancy site, and specific heat C_p compare favorably to the experimental measurements.

To evaluate the vacancy-formation energy E_v^f we first obtain the binding energy per atom. We note that this value is obtained by dividing the total energy by, in this particular case, 255 atoms for a MD cell with one vacancy. For a perfect crystal, we would divide the total energy by 256. Now we have the energy per atom for both systems and their difference times 256 is just the formation energy in our definition.

In estimating the vacancy-migration energy E_v^m, we follow the method suggested by Matthai[19] and measure

TABLE I. EAM calculation and experimental results on Ni bulk and surface properties.

	EAM calc.	Expt.
Lattice constant a_0 (a.u.)[c]	3.52	3.54
Cohesive energy E_b (eV)[c]	4.42	4.45
Vacancy-formation energy E_v^f (eV)	1.50	1.60
Vacancy migration energy E_v^m (eV)	1.2	1.3
Divacancy E_{2v}	2.89	
Heat capacity C_p (R)	3.0	3.0
Surface energy E_σ (ergs/cm^2)	3028 (100)[b]	
	3228 (110)	2380[a]
	1200 (111)	
Surface relaxation $\Delta_{1\text{-}2}$ (%)	−1.0 (100)	small
	−3.7 (110)	−4.1 → −8.3
	−0.8 (111)	small
$\Delta_{2\text{-}3}$ (%)	+0.1 (100)	
	+0.2 (110)	
	−0.1 (111)	

[a]Average over three surfaces.
[b](hkl) face in usual crystallographic notation.
[c]Properties calculated at simulation temperature $T=20$ K. Others measured at 300 K.

the T-dependent change in the number of time steps needed for an atom move into the vacancy region, identified by a circle of radius equal to half of the distance between the atomic site and the vacancy. According to statistical theory, the dependence of migration energy on this number of steps is

$$N = C(kT)^{1/2} e^{E_v^m/kT} \left[\frac{kT}{E_v^m} - 1 \right]^{1/4} . \quad (7)$$

After we tested the Ni potential on bulk potentials, we applied this model to the studies of surface relaxation and reconstruction of Ni (100), (110), and (111) surfaces, using a unit cell of 992 atoms in 31 layers. We chose the size of the MD cell with a minimum number of atoms consistent with a relatively stable simulation structure. From test runs we found that a cell with eight atoms in the x-y plane and 101 layers is greatly affected by the thermal fluctuations. Compared to the simulation on the nickel bulk, it is obvious a larger number is needed to sustain the stability of the dynamics under the influence of the temperature because of the lack of symmetry in the z direction. For all three surfaces we find little evidence of reconstruction, consistent with experimental reports on nickel low-index surfaces.[20] Figure 1 shows the predicted oscillatory relaxation of interlayer spacing. The (110) surface has a 3.5% contraction with respect to bulk spacing for the first layer, with a second-layer expansion of 0.1%. This compares well with the experimental results of -4.0% to -8.7%, and $+2.3\%$ changes of first and second interlayer spacing, respectively.[21] The relaxation of the other two surfaces, (100) and (111), is very small: -0.03% and -0.8% for (100) first two layers and -0.1% and -0.2% for (111). This is also consistent with previous measurements.[20] The slight systematic shift in the calculated interior interlayer spacing relative to bulk is found to be mainly due to thermal effects and finite film thickness in our model.

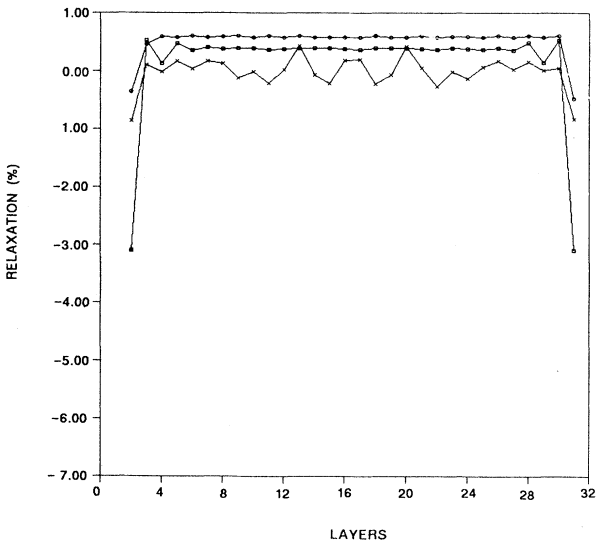

FIG. 1. Surface relaxation obtained by molecular-dynamics simulations on (a) Ni(100), ○; (b) Ni (110), □; (c) Ni(111), ×. The horizontal axis represents positions of layers in a finite-thickness film; the vertical axis gives the percentage deviation from the bulk value.

We also estimate the surface energy E_σ which is defined as the energy per unit area needed to separate two half-crystals to infinite distance. In our simulations E_σ is derived from the difference between bulk energy and film energy, i.e.,

$$E_\sigma = [E_{\text{bulk}}(\text{per atom}) - E_{\text{surf}}(\text{per atom})] \times \frac{\text{number of atoms in the film cell}}{2 \times (\text{area of the cell})} . \quad (8)$$

The results obtained by the simulation are 3028, 3228, and 1200 ergs/cm^2 for nickel (100), (110), and (111) surfaces, respectively. We may compare these to the experimental result of 2380 ergs/cm^2, averaged over all three surfaces.[22] It is remarkable that such a simple model potential is capable of producing both bulk and surface properties so consistent with the experimental results. The potential functions for the surface studies can be improved, in general, by taking the electron-density relaxation into account in generating $F(\rho)$, but in the present film calculations on nickel we see that the bulk-derived potentials are accurate enough within experimental sensitivity.

B. Construction of Fe potential functions and simulation on Fe systems

Our goal here is to construct Fe potentials, which have not been previously obtained with much success (after the present work was completed, a newly parametrized potential was reported by Harrison[15] which appears to be a considerable improvement on previous efforts) and apply them to the MD simulations. The effective pair interaction function ϕ_{ij} is extracted from the LD (Ref. 23) calculations in the Fe and Ni tetrahedral clusters. In order to determine ϕ_{ij} we calculated the total self-consistent binding energy as a function of the atomic separation and divided this energy by the number of interatomic bonds. The pair potential in the EAM scheme is then obtained by Eq. (3); we have explicitly

$$\phi_{\text{Fe-Fe}} = \phi^{\text{LD}}_{\text{Fe-Fe}} - \phi^{\text{LD}}_{\text{Ni-Ni}} + \phi^{\text{EA}}_{\text{Ni-Ni}} , \quad (9)$$

where ϕ is the effective two-body interaction defined both in LD theory and the EA method and the subscripts refer to different materials.

The embedding energy $F(\rho)$ is derived by combining Eqs. (3) and (4), as discussed above. We plot the functions $\phi_{\text{Fe-Fe}}$, $\phi_{\text{Ni-Ni}}$, and $\phi_{\text{Fe-Ni}}$ in Fig. 2. The differences between Fe and Ni are essentially that the pair potential for Fe has a negative region representing attraction while Ni is purely repulsive. The derived F function of Fe given in Fig. 3 is positive at small ρ, while for Ni the F function is always negative.[12] Whether or not the slight positive value of the iron embedding function at very small densities relates to the real physical interaction is not very important, because of the nonuniqueness of the

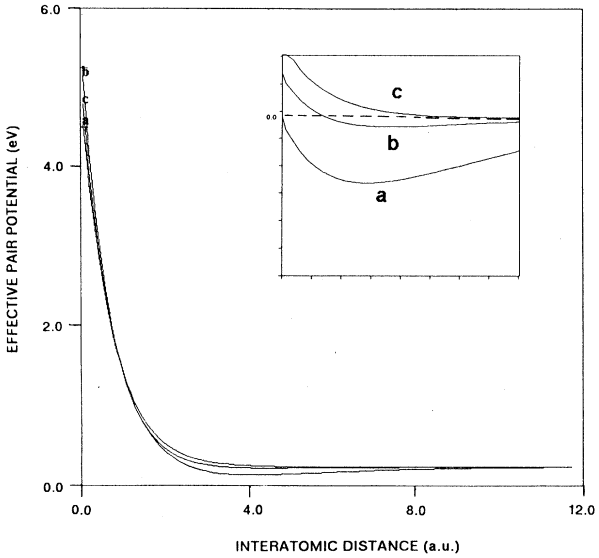

FIG. 2. Effective pair potential (a.u.) for Fe, Ni, and Fe_xNi_{1-x} systems. (a), Fe-Fe interaction; (b), Fe-Ni interaction; (c), Ni-Ni interaction. The horizontal axis represents the interatomic distance.

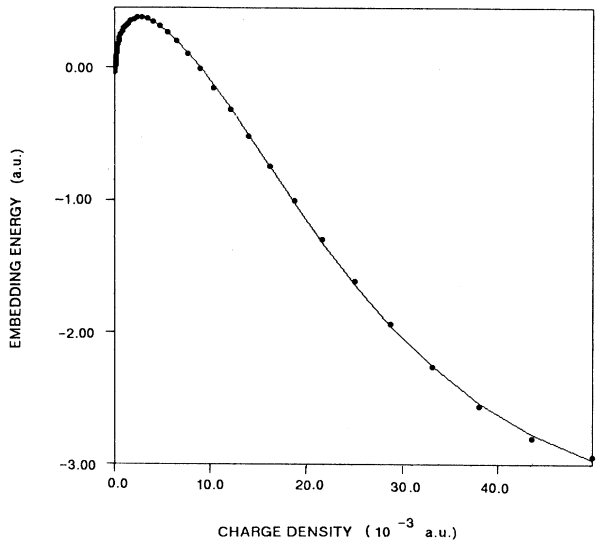

FIG. 3. The embedding energy (a.u.) as a function of the local charge density (a.u.) for iron obtained from the cohesive energy function of the bcc phase.

ϕ,F representation. It also does not seriously affect the bulk or surface simulation because such small ρ values appear only for dilute systems.

By analyzing the data we see that the potential functions generate bulk Fe properties consistent with experiment and the accuracy of the data is about the same as for bulk Ni (see Table II). For most of the simulation runs on Fe bulk and surfaces the temperature is kept at 300 K to match the room-temperature condition and zero external pressure. The vacancy-formation energy is found to be 2.1 eV, slightly higher than the 1.6 eV found from previous theoretical estimates and some experimental measurements.[24] However, Schepper *et al.*[25] report that for the ferromagnetic Fe crystal the value of E_v^f is higher than that for paramagnetic Fe; their data show a 2.0 ± 0.2 eV vacancy-formation energy. In our studies, the magnetic effects are only included implicitly through $\Delta\phi^{\mathrm{LD}}$ with no explicit dependence on spin in potential expressions. We measure the vacancy-migration energy E_v^f at the temperature 300 K and find a value of 0.65 eV [Eq. (7)]. We also find that the number of time steps diverges at 290 K, e.g., the migration is forbidden by the classical dynamics. The experimental measurements on E_v^m are controversial, with values ranging from 0.55 to 1.2 eV.[24]

TABLE II. EAM calculation and experimental results on Fe bulk and surface properties.

	EAM calc.	Expt.
Lattice constant a_0 (a.u.)	5.43	5.44
Cohesive energy E_b (eV)	4.28	4.28
Vacancy-formation energy E_v^f (eV)	2.04	1.60–2.0
Vacancy-migration energy E_v^m (eV)	0.65	0.55–1.2
Heat capacity C_p (R)	3.0	3.0
Surface energy E_σ (ergs/cm^2)	3550 (100) 4590 (110) 12 870 (111)	
Surface relaxation $\Delta_{1\text{-}2}$ (%)	16.0 (100) 6.0 (110) 33.0 (111)	
$\Delta_{2\text{-}3}$ (%)	6.0 (100) 0.4 (110) 18.0 (111)	

The simulation by Gibbsian dynamics on bcc iron surfaces were not very successful with the potential constructed from our method and the chosen atomic configuration for the host density, which was taken as the LD atomic Fe d^6s^2 state. The thin film is found to be squeezed in the x,y direction and expanded in the z (stacking) direction as a result of the Gibbsian dynamics which allows the size of the cell to vary under the external pressure P. We speculate that the causes of this failure may be mainly due to differences between the potentials derived from corrections to fcc bulk Ni for bulk Fe and the requirements of the dilute bcc surface structure. We recall that, in general, the empirical EAM potentials have been found to work better in the fcc metals than bcc metals. Improvements in Fe surface potential can doubtless be made for future simulations, but for the present we simply chose to freeze the box-size degree of freedom.

The disadvantage of the fixed-volume simulation is that some possible reconstruction on the surfaces may be missed due to the constraints. The calculated relaxations on all three surfaces—(100), (110), and (111)—are then found to be larger than for nickel. The overall systematic shift with respect to bulk is also quite large due to finite size and thermal effects. A significant difference between iron and nickel is that the first interlayer spacing increases for Fe while it contracts for Ni (see Fig. 4). In Table III we list the details of the calculated results.

We also treated the pair potential obtained directly from the Fe dimer LD binding-energy calculations, making corresponding adjustments to $F(\rho)$. As was found previously for Ni, the results on the vacancy-formation and -migration energies imply that the strength of the pair interaction is overestimated by the dimer potential. The calculated vacancy-formation energy is about 1.0 eV higher than the one resulting from the tetrahedral cluster two-body potential, which was already perhaps a bit high. This suggests again that we can improve the effective pair potential by considering large clusters, such as the Fe_{19} bcc fragment. However, the tetrahedral clusters have already provided excellent accuracy for certain properties, and it could be just as useful to refine the mean field further by modifying the atomic density distribution used in $F(\rho)$.

C. Potential functions and simulations of Fe-Ni alloys

Next, we build up the potential functions of iron-nickel alloys and impurity systems. By the EAM assumption, the $F(\rho)$ for Fe is invariant with respect to the host constituents, i.e., we use the same F for Fe in a Fe-Ni alloy as used in a pure Fe system. The pair interaction of Fe-Ni is derived from the two tetrahedra, a Ni_4 and a $FeNi_3$ cluster. The total binding energies are calculated versus the interatomic distance for both clusters and the differences between the two cluster binding energies are taken as the total differences of the two effective pair potentials. After dividing the energy difference by the number of Fe—Ni bonds, 3, we get the differences of the pair potential as a function of distance which is needed to obtain $\phi^{EA}_{Fe\text{-}Ni}$ in Eq. (9) (see Fig. 2).

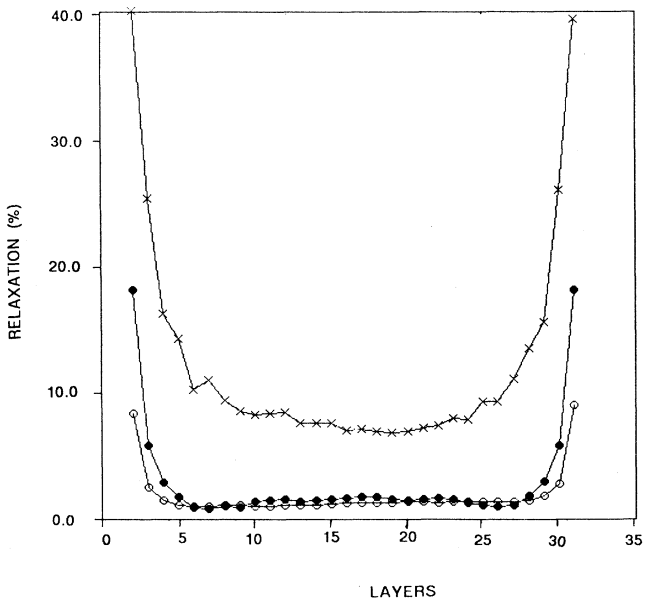

FIG. 4. Surface relaxation obtained by molecular-dynamics simulations on (a) Fe(100), ●; (b) Fe (110), ○; (c) Fe(111), □. The horizontal axis represents positions of layers in a finite-thickness film; the vertical axis gives the percentage deviation from the bulk value.

TABLE III. Calculated interlayer spacing (a.u.) near (hkl) surfaces for Ni, Fe, and Fe-covered Ni. The simulation temperature was $T=300$ K.

Layer Fe	(100)	(110)	(111)
1	3.21	4.15	2.20
2	2.87	3.93	1.96
3	2.80	3.90	1.82
4	2.76	3.87	1.78
bulk	2.76	3.87	1.67
Ni	**(100)**	**(110)**	**(111)**
1	3.31	2.29	3.85
2	3.34	2.38	3.87
3	3.34	2.37	3.88
4	3.34	2.38	3.88
bulk	3.35	2.37	3.88
Fe/Ni	**(100)**	**(110)**	**(111)**
1	3.42	2.42	cluster[a]
2	3.29	2.33	3.91
3	3.35	2.36	3.89
4	3.34	2.38	3.88
5	3.34	2.38	3.88
bulk	2.35	2.37	3.88

[a]Iron is found to form irregular clusters on the surface of the Ni substrate.

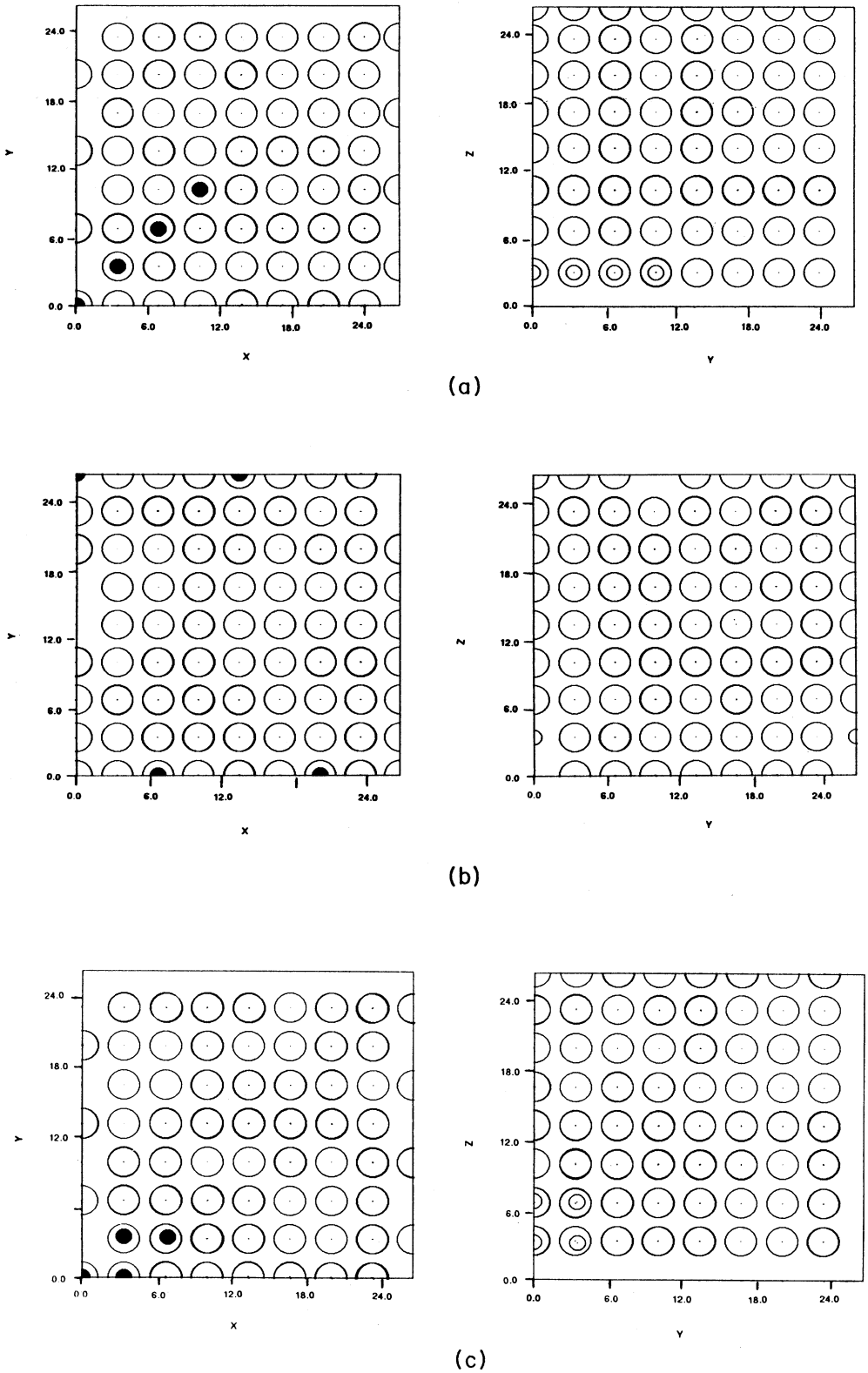

FIG. 5. Typical distributions from different reference planes: Equilibrium atomic position for Fe_4 clusters embedded in bulk nickel indicates no visible distortion from fcc structure. Figures display both x-y and y-z planes; small circles denote Fe atoms.

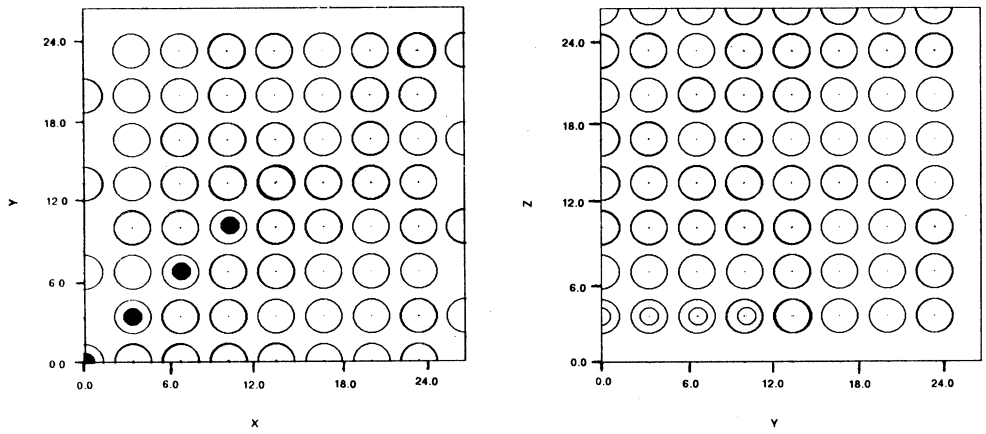

(d)

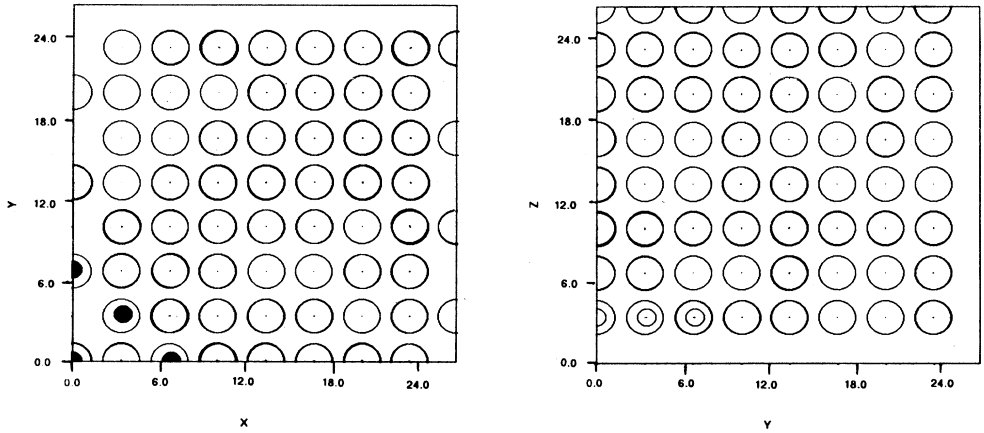

(e)

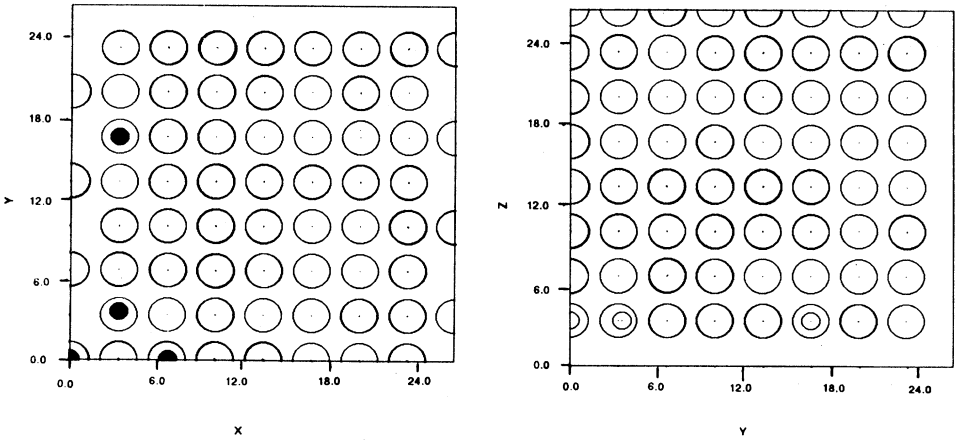

(f)

FIG. 5. (*Continued*).

With Fe-Fe, Fe-Ni, and Ni-Ni potentials, we investigated various types of Fe-Ni alloys, mostly nickel-rich cases. For such systems reasonably close to the fcc Ni "calibration point" the EAM is expected to provide a better description of the potential-energy surface than it does in the bcc structure. The tetrahedral clusters used in our LD calculations also provide a nickel-rich environment.

1. *Dilute $Ni_{1-x}Fe_x$ alloy*

In the first part of the calculations the iron atoms were embedded in the nickel bulk with the concentration 4:252. We studied their equilibrium states and diffusion in the bulk and found that at room temperature there is no visible diffusion over a simulation interval of 2000 time steps. The cohesive energy per atom decreased to 4.39 from the pure bulk nickel value of 4.45 eV/atom. The Gibbsian minimum-energy criterion determines the most stable cluster configuration: four Fe atoms occupying one of the corners of the fcc lattice cell. This indicates that the Fe atoms tend to cluster in bulk nickel at room temperature. Figure 5 illustrates by a "snapshot" some of the typical distributions found from different reference planes.

2. *Fe-Ni defect complexes*

We also studied a series of Ni and Fe defect structures, in bulk and dilute $Ni_{1-x}Fe_x$ alloys with formation energies listed in Table IV. Again we calculated the formation energies by the subtraction procedure discussed before. In order to have a consistent comparison all the simulations are done at zero pressure and $T=300$ K. The results display a consistent trend from single vacancy to substitutional structures. In the divacancy structure, we let the two vacancy sites be initially separated by a distance equal to the lattice constant at that temperature. The energy needed to produce such a vacancy pair is equal to 2.89 eV, almost twice the single vacancy energy. The divacancy formation energy for Fe bulk is also approximately twice the single vacancy energy. It can be seen that the energy required to generate a V_{Ni}-Fe pair as neighbors in Ni is larger than that for the Fe-Fe impurity cluster, but less than that for a divacancy. This is reasonable since Fe impurities will recover part of the intermetallic binding energy. The relaxation of the atoms around the Ni vacancy site, $\Delta a/a < 0.1$, is smaller than that predicted in pure bulk iron. This phenomenon is surely due to the difference of the crystal structure of the two bulk metals. The bcc structure is much more open than the fcc structure and it is thus more flexible to relax around the vacancy. There is no visible deformation around Fe site(s) when it (they) replace Ni atoms in the fcc structure.

TABLE IV. Calculated formation energies of various defect structures (eV).

	Bulk Ni	
Single vacancy	V	1.50
Divacancy	V-V	2.89
Vacancy-Fe pair	V-Fe	2.28
2 Fe atoms	Fe-Fe	1.51
	Bulk Fe	
Single vacancy	V	2.04
Divacancy		4.22

3. *Fe overlayers, sandwiches, and ordered alloys*

(a) Overlayers. Another aspect of our simulation experiments on the Fe-Ni alloys is the investigation of a monolayer iron film on the three low-index nickel (hkl) surfaces (100), (110), and (111). The unit box in our simulation contains 992 atoms. The top surface is covered by 32 Fe atoms which are initially located at the nickel sites while the bottom surface of the thin film still consists of nickel atoms. The temperature is kept at 300 K and the external pressure is zero during the simulations. We observe that Fe atoms form monolayer films on both Ni(100) and (110) surfaces and these films are commensurate with the substrates. However, the Fe atoms do not form a stable film on the Ni(111) surface at all but rather cluster together (see Figs. 6 and 7). The presence of the surface Fe atoms also influences the first and second nickel layers; Fig. 8 shows the resulting relaxation on the three surfaces. The asymmetric patterns of the interlayer spacing reflect the significant difference between pure-nickel- and iron-covered surfaces. For each case the surface structures rearrange themselves to lower the total Gibbsian energy, and in order to understand these results better we analyze the different contributions to the total energy and illustrate the results in Table V. The first column gives the Fe-Fe interaction on the surface layer. It is clear that the Fe forms (100) and (110) surfaces with Fe-Fe negative pairwise energies of -8.5 and -10.4 eV, respectively, and that relaxation stabilizes the Fe-Fe interaction energies further. The reason for the clustering of Fe atoms on the (111) surface is now quite evident since the unrelaxed surface has a very high positive value of Fe-Fe potential energy. This part of the energy decreases from $+6.2$ to -27.2 eV as a result of the surface atom rearrangement. The other columns include the embedding energies of two elements and different layers, and the strength of the interactions between different layers (note that the data given in the table refer to the total energy, not energy per atoms). The embedding energy $F(\rho)$ in (111) planes regains part of the energy due to the increase in local charge density, but the total Gibbsian energy still decreases with respect to the unrelaxed lattice. For all three types of planes the embedding energies of the different nickel layers show a slight oscillation near the surface. The interlayer spacing for the first few layers and the center of the film have been given in Table III for comparison to the pure-nickel surfaces.

The influence of four- and eight-Fe-atom coverage on the nickel (100) surface (corresponding to surface coverages $\frac{1}{8}$ and $\frac{1}{4}$) was studied by embedding Fe atoms initially at the nickel lattice sites. Their equilibrium structures

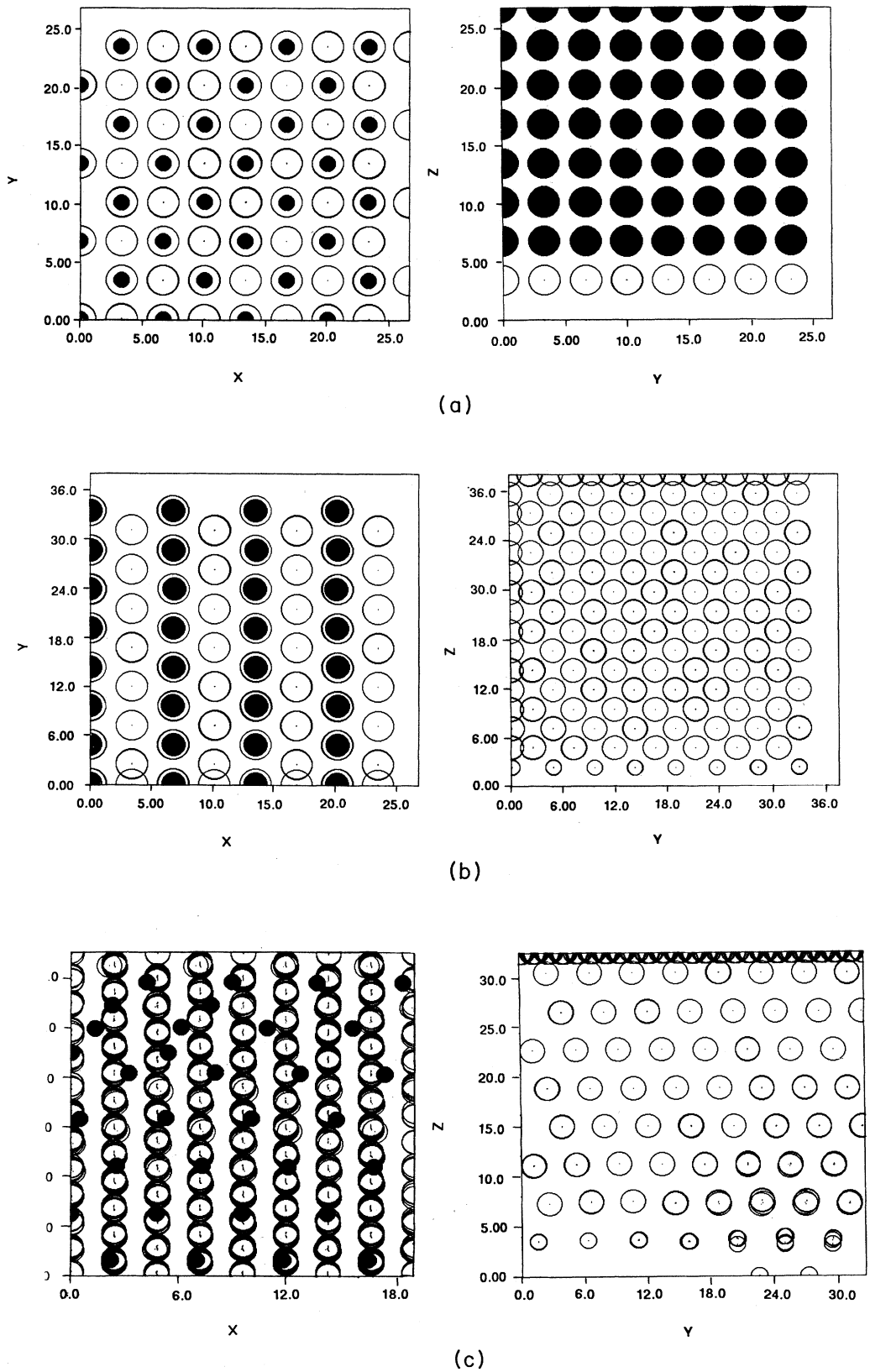

FIG. 6. Equilibrium atomic position for Fe monolayer on (a) Ni(1000), (b) Ni(110), and (c) Ni(111) surface. There is no visible distortion from fcc structure. Figures display both *x-y* and *y-z* planes; small circles denote Fe atoms.

on the surface were examined. We conclude that the Fe atoms are stable in the nickel lattice sites on the (100) plane. The surface energies are increased by 11% and 26% as shown in Table VI. In general, the presence of Fe increases the surface energy, destabilizing the surface and causing slight contraction of the lattice. This effect scales uniformly with the Fe concentration in the alloys.

(b) Sandwiches and ordered alloys. The atom distribution of an Fe monolayer within the bulk nickel (a sandwich) indicates a good commensuration on the two sides of the Fe layer. The energy cost of inserting the Fe monolayer is estimated by comparing the total-energy difference between the two systems. The concentration of the alloy was chosen as Fe:Ni=32:224. In Table VI we give the data on the lattice constants and "cohesive energies" of the above alloys.

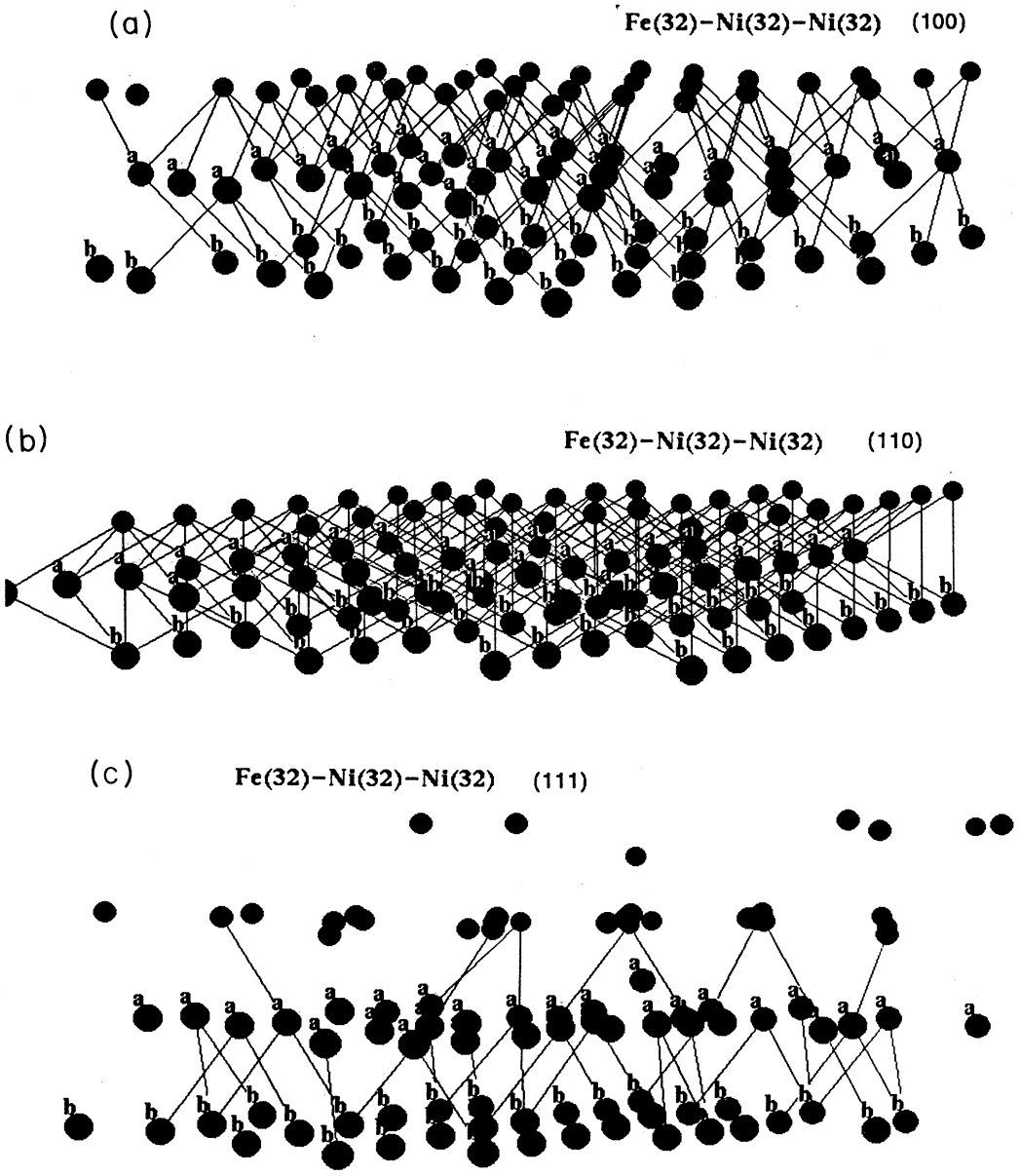

FIG. 7. Side view of Fe-covered Ni surfaces, Fe and two Ni layers are drawn. Fe forms a monomolecular film which is commensurate with the substrate in (a) [100] and (b) [110], but not in (c) [111] directions.

TABLE V. EAM energy analysis of Fe-monolayer covered Ni surfaces, obtained, layer energies in eV. The asterisk denotes an unrelaxed surface model.

	By layer-by-layer summed pair interactions: $\sum_{i,j}\phi_{ij}$ (atom in i,j layer)				
ϕ_{ij}	Fe	Ni(1)	Ni(2)	Ni(3)	Ni(4)
	−8.5	38.1	−3.6	0.2	0.0 Fe on Ni (100)
Fe	−10.4	43.5	6.7	2.0	0.2 Fe on Ni (110)
	−27.2	24.6	−1.6	0.0	0.0 Fe on Ni (111)
		35.2	73.8	0.6	0.0
Ni(1)		19.0	72.5	19.0	0.1
		53.0	52.2	0.1	0.0
			35.2	68.9	0.5
Ni(2)			19.0	70.3	17.2
			53.5	51.7	0.1
				35.2	69.2
Ni(3)				19.0	69.4
				53.5	52.0
					35.2
Ni(4)					18.8
					53.4

ϕ^*_{ij}	Fe	Ni(1)	Ni(2)	Ni(3)	Ni(4)
	−6.5	46.0	−3.6	−0.2	0.0
Fe	−10.2	47.8	8.5	2.0	0.3
	6.2	30.2	−0.2	0.1	0.0
		35.2	73.8	0.6	0.0
Ni(1)		18.9	72.4	19.0	0.1
		53.4	55.4	0.1	0.0
			35.2	68.9	0.5
Ni(2)			18.9	72.4	19.0
			53.4	55.5	0.1
				35.2	69.2
Ni(3)				18.9	72.4
				53.4	55.4
					35.2
Ni(4)					18.9
					53.4

	Summed pairwise interactions between different atom types (eV)		
(hkl) surface	$\sum\phi_{\text{Fe-Fe}}$	$\sum\phi_{\text{Fe-Ni}}$	$\sum\phi_{\text{Ni-Ni}}$
(100)	−8.5	34.7	3084.5
(100)*	−6.5	42.2	3232.2
(110)	−10.4	52.7	3067.0
(110)*	−10.2	58.6	3194.4
(111)	−27.2	23.0	3110.6
(111)*	6.2	30.1	3212.3

	Embedding energy $F(\rho)$ for each layer (eV)				
	Layer				
(hkl) surface	1	2	3	4	5
(100)	−47.1	−266.2	−250.4	−246.9	−247.1
(100)*	−47.1	−272.1	−253.8	−252.3	−252.3
(110)	−37.7	−255.8	−255.2	−248.5	−246.6
(110)*	−37.2	−258.3	−258.8	−252.9	−252.3
(111)	−34.8	−254.9	−247.5	−247.4	−247.5
(111)*	−57.9	−270.7	−251.6	−250.1	−250.1

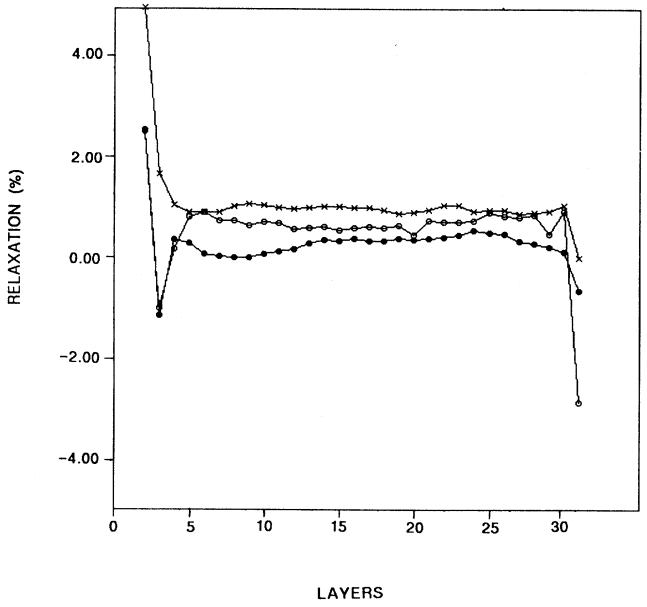

FIG. 8. Surface relaxation obtained by molecular-dynamics simulations on Fe-covered (a) Ni(100), ●; (b) Ni(110), ○; (c) Ni(111), ×. The horizontal axis represents positions of layers in a finite-thickness film; the vertical axis gives the percentage deviation from the bulk value.

In order to test the validity of the presently obtained potential function further, we studied a 50%-50% Fe-Ni bulk alloy in which Fe and Ni atoms are initially randomly distributed in the crystal. Both fcc and bcc structures were tested and the results indicated that fcc is more stable than bcc, with cohesive energy 4.21 and 4.19 eV, respectively (Table VII). For a $Fe_{0.4}$-$Ni_{0.6}$ alloy the cohesive energy for fcc structure is 4.20 eV. A $Fe_{0.5}$-$Ni_{0.5}$ layer structure was also simulated by our model potential in a fcc crystal array, formed by alternating Fe and Ni slabs. We find that Fe atoms are quite stable in fcc sites, with a cohesive energy and bond length of 4.19 eV and 6.78 a.u., respectively.

IV. CONCLUSION AND DISCUSSION

From the results presented here, we conclude that methods of construction of the potential-energy function described in this paper provide a viable way to apply *ab initio* methods to correct and extend empirical models. Our potential functions produce a number of physical properties which agree with experimental values to a reasonable accuracy, when applied to various iron, nickel, and alloy systems. It is seen that this method does not work as well on the Fe surface as on the Ni surfaces and Fe-covered Ni surfaces, because of the relatively open structure of bcc metals. The failure on Fe surfaces may come from several sources:

(i) the well-known EAM tendency to produce better results for the more closely packed fcc structure;

(ii) the non-negligible relaxation of atomic charge density near the surface;

(iii) large MD cells are needed to reduce thermal effects.

We believe that, in principle, we can improve the EAM used in the present study by improving the charge-density evaluation used as an input to the embedding function. For example, instead of using $\rho(r_0)$ we can average $\rho(r)$ over a small region around each reference point, and we can optimize the effective atomic configurations. Concerning the second problem discussed above, we can parametrize the charge density as a function of distance from the surface. The limitation on cell size is straightforward, but the solution depends greatly on available computer facilities. Fortunately, modern supercomputers are well qualified to simulate a system of 10^4 particles and time intervals orders of magnitude greater than were treated here. Although our investigation does not yet address problems concerning macroscopic dislocations, grain boundaries, and certain ordered alloy structures, we believe that results obtained justify further application of our model potentials to such problems.

TABLE VI. EAM calculated surface and interface energies for various $Ni_{1-x}Fe_x$ interfaces. $T=300$ K.

$Ni_{1-x}Fe_x$		E_σ (ergs/cm^2)	a_0 (a.u.)
Ni_{992}	(100)	1488	6.67
$Ni_{988}Fe_4$	(100)	1654	6.65
$Ni_{984}Fe_8$	(100)	1869	6.65
$Ni_{960}Fe_{32}$	(100)	5070	6.67
$Ni_{224}Fe_{32}$	(100)[a]	4231	6.70
$Ni_{960}Fe_{32}$	(110)		6.67
$Ni_{960}Fe_{32}$	(111)		6.67

[a]Fe monolayer sandwiched in bulk Ni.

TABLE VII. Calculated lattice constant and cohesive energies of Fe-Ni alloys ($T=300$ K).

Fe_xNi_{1-x}	a_0 (a.u.)	E_{sub} (eV)
$Fe_{128}Ni_{128}$[a] (fcc)	6.72	4.20
$Fe_{128}Ni_{128}$[a] (bcc)	6.67	4.18
$Fe_{32}Ni_{224}$	6.70	4.29
$Fe_{128}Ni_{128}$	6.78	4.19
$Fe_{100}Ni_{156}$	6.71	4.20
Fe_4Ni_{252}	6.68	4.39
Fe_2Ni_{254}	6.68	4.39
Fe_1-$V$$Ni_{254}$	6.68	4.39
V-$V$$Ni_{254}$	6.68	4.39
V-$V$$Fe_{248}$	5.43	4.20

[a]Ni-Fe 50:50 alloy with substitutional disorder in sandwiches.

ACKNOWLEDGMENTS

This work was supported by the U.S. National Science Foundation through the Northwestern University Materials Center under Grant No. DMR-85-20280. A part of the calculations was carried out at the National Center for Supercomputing Applications (Urbana, IL).

[1]W. Rosehain, in *An Introduction to Physical Metallurgy* (Constable, London, 1914); *The Sorby Centennial Symposium on the History of Metallurgy,* edited by C. S. Smith (Gordon and Breach/AIME, New York, 1965); C. S. Smith, in *Metallurgy as a Human Experience* (ASM, Metals Park, OH/AIME, New York, 1977); *Dictionary of Scientific Biography,* edited by C. C. Cillispie (Scribner's, New York, 1970–1980).

[2]O. G. Pettifor, in *Physical Metallurgy,* edited by R. W. Cahn and P. Haasen (North-Holland, Amsterdam, 1983), Chap. 3; H. Biloni, *ibid.*, Chap 9; H. J. Wollenberger, *ibid.*, Chap. 17.

[3]G. D. Mahan, *Many-Particle Physics* (Plenum, New York, 1981).

[4]P. Hohenberg and W. Kohn, Phys. Rev. **136**, B864 (1964); W. Kohn and L. J. Sham, *ibid.* **140**, A1133 (1965).

[5]*Computer Simulation in Physical Metallurgy,* edited by Gianni Jacucci (Reidel, Dordrecht, 1986).

[6]B. Delly, D. E. Ellis, and A. J. Freeman, Phys. Rev. B **27**, 2132 (1983); G. F. Holland, D. E. Ellis, and W. C. Trogler, J. Chem. Phys. **83**, 3507 (1985).

[7]J. N. Murrell *et al.*, *Molecular Potential-Energy Functions* (Wiley, Chichester, 1984); M. J. Stott and E. Zaremba, Phys. Rev. B **22**, 1564 (1980).

[8]J. K. Norskøv and N. D. Lang, Phys. Rev. B **21**, 2131 (1980); M. J. Stott and E. Zaremba, Solid State Commun. **32**, 1297 (1979).

[9]M. S. Daw and M. I. Baskes, Phys. Rev. B **29**, 6443 (1984).

[10]S. M. Foiles, Phys. Rev. B **32**, 3409 (1985); *ibid.* **32**, 7685 (1985).

[11]S. M. Foiles, M. I. Baskes, and M. S. Daw, Phys. Rev. B **33**, 7983 (1986).

[12]M. S. Daw and S. M. Foiles, J. Mater. Res. **2**, 5 (1987).

[13]F. Voter and S. P. Chen, in *Materials Research Society Symposium Proceedings* (MRS, Boston, 1987), Vol. 82, p. 174.

[14]J. R. Smith, J. Ferrante, and J. H. Rose, Phys. Rev. B **25**, 1419 (1982); **28**, 1835 (1983); **29**, 2963 (1984); D. Spanjaard and M. C. Desjonqueres, *ibid.* **30**, 4822 (1984).

[15]R. J. Harrison, A. F. Voter, and S.-P. Chen (unpublished).

[16]H.-P. Cheng and D. E. Ellis (unpublished).

[17]F. F. Abraham, S. W. Koch, and W. E. Rudge, Phys. Rev. Lett. **49**, 1830 (1980); D. J. Evans and G. P. Morris, Chem. Phys. **77**, 63 (1983); F. F. Abraham, W. E. Rudge, D. J. Auerbach, and S. W. Koch, Phys. Rev. Lett. **52**, 255 (1984); S. Nosé, Mol. Phys. **52**, 255 (1984); W. G. Hoover, Phys. Rev. A **31**, 1695 (1985).

[18]H.-P. Cheng, Ph.D. thesis, Northwestern University, Evanston, IL, 1988.

[19]C. C. Matthai, Philos. Mag. A **52**, 305 (1985).

[20]See Refs. 9 and 11.

[21]D. L. Adams and L. E. Peterson, and C. S. Sorensen, J. Phys. C **18**, 1753 (1985).

[22]W. R. Blakely and G. A. Samorjai, Surf. Sci. **62**, 267 (1977).

[23]W. Kohn and P. Vashishta, in *Theory of the Inhomogeneous Electron Gas* (Plenum, New York, 1983); W. Kohn and L. J. Sham, Phys. Rev. **140**, A1133 (1965); D. E. Ellis and G. S. Painter, Phys. Rev. B **2**, 2887 (1970); T. Parameswaran and D. E. Ellis, J. Chem. Phys. **58**, 2088 (1973); E. J. Baerends, D. E. Ellis, and P. Ros, Chem. Phys. **2**, 41 (1975).

[24]*Physical Metallurgy,* edited by R. W. Cahn and P. Haasen (North-Holland, Amsterdam, 1983), Chap. 17.

[25]L. De Schepper, G. Kauyt, L. M. Stals, and P. Moser, Phys. Rev. B **27**, 5257 (1983).